Demethylase FTO attenuates atherosclerotic plaque via upregulating ABCA1 and ABCG1 expression by targeting ATG5

FENGXIA GUO[1], MEI HE[2], YAONAN LI[3], KANGNING ZHU[1] and BING HU[4]

[1]Department of Clinical Laboratory, Henan Provincial People's Hospital, People's Hospital of Zhengzhou University, Zhengzhou, Henan 450003, P.R. China; [2]Zhengzhou No. 7 People's Hospital, Zhengzhou, Henan 450016, P.R. China; [3]Department of Emergency, Henan Provincial People's Hospital, People's Hospital of Zhengzhou University, Zhengzhou, Henan 450003, P.R. China; [4]Department of Clinical Laboratory, Affiliated Cancer Hospital of Zhengzhou University, Zhengzhou, Henan 450003, P.R. China

Received December 5, 2025; Accepted June 16, 2026

DOI: 10.3892/mmr.2026.14025

Abstract. N6-methyladenosine (m^6A), the predominant internal modification in eukaryotic mRNAs, has emerged as a significant epigenetic regulator in atherosclerosis; however, its precise mechanistic contributions remain inadequately elucidated. The present study demonstrated that the m^6A demethylase fat mass and obesity-associated (FTO) regulates autophagy, lipid metabolism and plaque vulnerability by targeting autophagy related 5 (ATG5). FTO knockdown resulted in reduced ATG5 expression, thereby suppressing autophagy and downregulating ATP-binding cassette transporter A1 (ABCA1) and ATP-binding cassette sub-family G member 1 (ABCG1). The regulation of ATG5 expression by FTO occurs through direct binding to its transcripts as well as m^6A-mediated mechanisms. Increased m^6A modification on ATG5 mRNA following FTO silencing enhanced its recognition by YTH domain-containing family 1, leading to transcript degradation and diminished protein levels. Consequently, autophagy and cholesterol efflux pathways were inhibited. *In vivo* experiments revealed that specific FTO knockdown compromised plaque stability and impaired ATG5-mediated autophagy, in addition to downregulating ABCA1 and ABCG1. These findings highlighted the FTO-ATG5-ABCA1/ABCG1 axis as a critical regulator of autophagy and lipid homeostasis in atherosclerosis.

Introduction

Atherosclerosis is a complex pathophysiological process that can lead to severe complications such as plaque growth, erosion, or rupture (1,2). Advanced plaques, characterized by a high density of macrophages and a low collagen content, are particularly susceptible to rupture. The subsequent release of inflammatory mediators from lipid-rich cores can trigger ischemic events, including myocardial infarction (3). Despite advances in prevention and treatment, coronary heart disease poses a significant global health burden. Patients experiencing acute coronary syndromes face considerable mortality risks, primarily due to thrombosis resulting from the rupture of unstable or erosion-prone plaques. Although intravascular ultrasound and optical coherence tomography are considered the gold standards for assessing plaque vulnerability, their invasive nature and procedural complexity restrict their practicality. Thus, the development of non-invasive strategies for the early identification of unstable plaques remains a critical clinical goal. Assessing plaque burden and lipid content is, therefore, fundamental for evaluating the progression and severity of underlying diseases.

N6-methyladenosine (m^6A), the most prevalent RNA modification in eukaryotes, serves as a key epigenetic regulator that influences mRNA processing, metabolism, secondary structure, subcellular localization, translation efficiency and degradation. Dysregulation of m^6A methylation has been observed in atherosclerotic lesions (4) and epidemiological studies have linked polymorphisms in the FTO gene (such as rs1421085, rs17817449 and rs1121980) to an increased risk of atherosclerosis (5). These variants correlate with established risk factors such as dyslipidemia and hypertension (6). However, a direct causal relationship between FTO dysfunction and plaque instability has yet to be established.

Autophagy, a conserved eukaryotic mechanism, is essential for maintaining cellular homeostasis and its dysregulation has been implicated in various pathologies, including cardiovascular disease (7,8). Macroautophagy, the predominant form, is regulated by epigenetic mechanisms, including m^6A RNA methylation (9). Specifically, FTO depletion enhances autophagy by suppressing MTORC1 signaling (10), although its ectopic expression reportedly does not influence starvation-induced autophagy (11). Furthermore, FTO has been found to increase ULK1 protein abundance and promote autophagy in an m^6A-dependent manner (12), emphasizing the context-specific regulatory roles of FTO. Thus, the mechanistic

Correspondence to: Professor Fengxia Guo, Department of Clinical Laboratory, Henan Provincial People's Hospital, People's Hospital of Zhengzhou University, 7 Weiwu Road, Zhengzhou, Henan 450003, P.R. China
E-mail: guoxia0312@163.com

Key words: fat mass and obesity-associated, atherosclerotic plaque, autophagy

interplay among m^{6}A, FTO and autophagy necessitates further exploration.

The present study investigated the role of FTO-regulated m^{6}A demethylation in mediating autophagy and lipid metabolism. Findings indicated that FTO critically modulates autophagy and lipid homeostasis by fine-tuning ATG5 expression through an m^{6}A-YTH domain-containing family (YTHDF) 1-dependent mechanism. Additionally, adipose-specific FTO knockdown impairs ATG5-dependent autophagy in mice. These results revealed the involvement of m^{6}A in autophagy regulation and identified a novel pathway through which m^{6}A methylation influences lipid metabolism via autophagy.

Materials and methods

All procedures adhered to the NIH guidelines (Publication No. 85-23, 1996 revision) (13) and received approval from the Animal Ethics Committee of Zhengzhou No. 7 People's Hospital (approval no. 2024-017). Male apolipoprotein E-deficient (ApoE$^{-/-}$) mice, aged six weeks and weighing 20 g, on a C57BL/6J genetic background (n=20), were obtained from the Laboratory Animal Center at Peking University. The mice were maintained in an environment with a controlled temperature of 23±1˚C and a relative humidity of 60±5%, under a 12-h light/dark cycle, with unrestricted access to food and water. To investigate the development of atherosclerosis, the ApoE$^{-/-}$ mice were randomly assigned to the following groups, with allocation concealment: i) Adeno-associated virus (AAV)-mock; ii) AAV-sh-FTO (n=10 per group). The high-fat diet (HFD) administered comprised 20% protein, 40% carbohydrate, and 40% fat (cat. no. D12108C; OpenSource diets; Research Diets, Inc.). The anesthetic administered was 1% pentobarbital sodium, with the dosage adjusted according to the animal's body weight (40 mg/kg) (13). Blood samples were obtained from the retro-orbital venous plexus utilizing a capillary tube. Subsequently, the mice were sacrificed by cervical dislocation, and tissues were harvested for histological and immunohistochemical analyses. These analyses were conducted in a blinded manner with respect to the group allocations of the animals.

Cell culture. THP-1 cells were cultured in RPMI 1640 medium (Beijing Solarbio Science & Technology Co., Ltd.) supplemented with 10% fetal bovine serum (FBS) and 2% penicillin-streptomycin, and maintained at 37˚C in a humidified incubator with 5% CO_2. To induce differentiation from monocytes to macrophages, the cells were treated with 160 nM phorbol 12-myristate 13-acetate for 24 h. Following differentiation, the macrophages were exposed to 50 μg/ml oxidized low-density lipoprotein (ox-LDL) for 48 h to facilitate foam cell formation. THP-1-derived foam cells were seeded into 24-well plates at a density of 1-3x10^5 cells per well and cultured overnight to achieve 60-80% confluence prior to transduction. The cells were transduced with either an empty vector control (LV-Mock) or LV-FTO, both obtained from Genechem Co., Ltd., Shanghai, China, at a multiplicity of infection (MOI) of 100, in the presence of 8 μg/ml polybrene (cat. no. PP101; Genechem). The viral transduction mixture was prepared using serum-free RPMI 1640 medium and subsequently added to the cells, which were then incubated at 37˚C in a 5% CO_2 humidified incubator for 24 h. Following the transduction process, the medium was replaced with fresh RPMI 1640 supplemented with 10% FBS, and the cells were cultured for an additional 48 h. The efficiency of transduction was verified through quantitative PCR analysis.

High-performance liquid chromatography (HPLC). Cholesterol quantification was conducted utilizing a reversed-phase HPLC system. This system comprised a PerkinElmer Flexar™ (PerkinElmer, Inc.) liquid chromatography apparatus, which was equipped with a UV-Vis detector and employed TotalChrom software (version 6.2; PerkinElmer, Inc.) for data acquisition and processing. Chromatographic separation was achieved using a Zorbax ODS column (dimensions: 4.6x250 mm, particle size: 5 μm; Agilent Technologies, Inc.). The column was maintained at ambient temperature (~25˚C). The mobile phase was composed of acetonitrile and isopropanol in a 50:50 volume ratio, delivered at an isocratic flow rate of 1.0 ml/min. An injection volume of 20 μl was utilized. The eluate was monitored at a UV wavelength of 210 nm. Cholesteryl heptadecanoate (17:0 cholesteryl ester) served as the internal standard. For the quantification of free cholesterol (FC), 0.4 units of cholesterol oxidase were added to each sample. Total cholesterol (TC) was measured by incubating samples with 0.4 units of cholesterol oxidase in conjunction with 0.4 units of cholesterol esterase. The content of cholesteryl esters (CE) was calculated as the difference between TC and FC (CE=TC-FC).

Cell transfection and RNA knockdown. Recombinant adenoviruses expressing mCherry-EGFP-LC3 (Ad-mCherry-EGFP-LC3) were obtained from Hanheng Biotechnology (Shanghai) Co., Ltd. For the study of adenoviral infections, cells were cultured in 6-well plates and exposed to the respective viruses for a duration of 48 h. In a similar experimental setup, short hairpin RNA (shRNA) transfections were performed utilizing the Lipofectamine® 3000 reagent (Thermo Fisher Scientific, Inc.), followed by an incubation period of 48 h. The shRNAs targeting FTO (shFTO), ATG5 (shATG5), YTHDF1 (shYTHDF1), YTHDF2 (shYTHDF2), and YTHDF3 (shYTHDF3), as well as a scrambled negative control shRNA (Scr-shRNA), were procured from Guangzhou RiboBio Co., Ltd. in the form of shRNA-expressing plasmid vectors. For the transfection process, cells were seeded in 6-well plates and transfected with 500 ng of shRNA plasmid per well, employing the Lipofectamine® 3000 reagent in accordance with the manufacturer's instructions. The transfection complexes were subsequently introduced to the cells and maintained at 37˚C for 48 h prior to further analysis. All procedures were carried out in strict accordance with the manufacturer's instructions.

The following primes (human) were used: Scr-shRNA: 5'-TTCTCCGAACGTGTCACGTTT-3'; shFTO: 5'-GGACTTAAGGAATCCAGAATT-3'; shATG5: 5'-GCTTCGAGATGTGTGGTTTTT-3'; shYTHDF1: 5'-GGACATTGGTACTTGGGATT-3'; shYTHDF2: 5'-GGGATTGACTTCTCAGCATT-3'; shYTHDF3: 5'-TAAGTCAAAGAAGACGTATTATT-3'.

Western blot analysis. Cell and tissue proteins were extracted utilizing RIPA lysis buffer (P0013B; Beyotime Biotechnology), augmented with a protease and phosphatase inhibitor cocktail (cP1045; Beyotime Biotechnology) while maintained on ice. Protein concentrations were quantified using a BCA Protein Assay Kit (P0012S; Beyotime Biotechnology). Total protein (~30 μg per sample) was subjected to separation via 10% SDS-PAGE, followed by transfer onto polyvinylidene difluoride membranes (MilliporeSigma; IPVH00010). After blocking with 5% bovine serum albumin (BSA; Beyotime Biotechnology) for 1 h at room temperature, the membranes were incubated overnight at 4˚C with primary antibodies: anti-FTO (cat. no. ab124892; Abcam; 1:1,000), anti-ABCA1 (cat. no. ab18180; Abcam; 1:200), anti-ABCG1 (cat. no. ab52617; Abcam; 1:1,000), anti-CD36 (cat. no. ab133625; Abcam; 1:1,000), anti-scavenger receptor A (SR-A) (cat. no. ab217843; Abcam; 1:500), anti-LC3 (ab192890; Abcam; 1:2,000), anti-p62 (cat. no. ab109012; Abcam; 1:5,000), anti-ATG7 (cat. no. ab52472; Abcam; 1:1,000), and anti-ATG5 (cat. no. ab108327; Abcam; 1:1,000). After three washes with TBST, membranes were incubated with horseradish peroxidase (HRP)-conjugated goat anti-rabbit secondary antibodies (cat. no. ab6721; Abcam; 1:10,000 dilution,) for 1 h at room temperature. Protein bands were visualized using an enhanced chemiluminescence (ECL) detection system (ChemiDoc; Bio-Rad Laboratories, Inc.). The protein expression levels were assessed in a semi-quantitative manner using ImageJ software (version 2.14.0/1.54f; National Institutes of Health), employing GAPDH as a reference control.

Immunofluorescence analysis. The sections underwent deparaffinization using xylene and a descending series of anhydrous ethanol, followed by rinsing with PBS. Antigen retrieval was performed using a sodium citrate buffer. Sections were incubated overnight at 4˚C with primary antibodies: The following primary antibodies were utilized: anti-CD31 (rabbit; cat. no. ab9498; Abcam) at a dilution of 1:100, anti-CD68 (rabbit; cat. no. ab283654; Abcam) at a dilution of 1:200, α-SMA (mouse; cat. no. A5228, MilliporeSigma) at a dilution of 1:500, and anti-FTO (rabbit; cat. no. ab280081; Abcam) at a dilution of 1:1,000. Subsequently, the sections were incubated with Alexa Fluor™ 488-conjugated goat anti-rabbit IgG (H+L) secondary antibody (A-11008, Thermo Fisher Scientific, Inc.) at a 1:500 dilution and Alexa Fluor™ 594-conjugated goat anti-mouse IgG (H+L) secondary antibody (cat. no. A-11005, Thermo Fisher Scientific, Inc.) at a 1:500 dilution for 1 h at room temperature. The nuclei were counterstained with DAPI (cat. no. D9542; MilliporeSigma) at a concentration of 1 μg/ml for 5 min at room temperature. Imaging was conducted using a Nikon A1R confocal microscope (Nikon Corporation), and subsequent analysis was performed using ImageJ software (version 2.14.0/1.54f, National Institutes of Health).

RNA immunoprecipitation-quantitative PCR (RIP-qPCR) analysis. RNA Immunoprecipitation (RIP) was conducted utilizing the PureBinding® RNA Immunoprecipitation Kit (P0101; Guangzhou Geneseed Biotech. Co., Ltd.) following the manufacturer's instructions. In summary, approximately $2x10^7$ cells were lysed in 405 μl of RIP Lysis Buffer, which was supplemented with protease and RNase inhibitors. A fraction of the lysate (10%) was set aside as the input control and stored at -80˚C. The remaining lysate was allocated into two groups: The immunoprecipitation (IP) group and the negative control IgG group. Protein A/G magnetic beads were incubated with 3-5 μg of anti-YTHDF1 antibody or normal rabbit IgG (as a control) in IP buffer at 4˚C overnight with gentle rotation. Following incubation, the beads underwent three washes with RIP Wash Buffer. The immunoprecipitated RNA and Input RNA were both subsequently purified via a column-based extraction technique and subjected to analysis through reverse transcription-quantitative PCR (RT-qPCR). The RT-qPCR was performed using the PowerUp™ SYBR™ Green Master Mix (A25742, Applied Biosystems; Thermo Fisher Scientific, Inc.) on an Applied Biosystems™ 7500 Real-Time PCR System (Thermo Fisher Scientific, Inc.). The thermocycling protocol included an initial denaturation step at 95˚C for 2 min, followed by 40 cycles of denaturation at 95˚C for 15 sec, annealing at 60˚C for 30 sec and extension at 72˚C for 30 sec. The relative enrichment of the target RNA was quantified using the $2^{-\Delta\Delta Cq}$ method (14), with normalization to the Input RNA.

Analysis of mRNA stability. Following a 36-h transfection period with either Scr-shRNA or shRNA targeting YTHDF1/FTO, cells were treated with 4 μM actinomycin D (MedChemExpress) to inhibit global transcription. After incubation for the specified durations, cells were harvested and total RNA was extracted for reverse transcription. The resulting cDNA was subjected to RT-qPCR to quantify target mRNA levels.

Assessment of atherosclerotic lesion. Paraffin-embedded heart valve tissues were sliced into 6-8 μm thick sections, stained with hematoxylin-eosin and Masson staining at room temperature for 5 min, and assessed for necrotic core areas and collagen content in atherosclerotic lesions using ImageJ software (version 2.14.0/1.54f; National Institutes of Health).

Immunohistochemistry (IHC). For the purpose of immunohistochemical staining, formalin-fixed, paraffin-embedded sections (4 μm thick) derived from mouse atherosclerotic plaques treated with AAV-sh-FTO or from cardiac arterial valve specimens transfected with a negative control were subjected to deparaffinization in xylene and subsequently rehydrated through a graded ethanol series. Antigen retrieval was conducted by heating the sections in citrate buffer (pH 6.0) at a temperature range of 95-100˚C for 20 min. Following a cooling period to room temperature, the sections were treated with 3% H_2O_2 in methanol for 10 min at room temperature to inhibit endogenous peroxidase activity. Subsequently, the sections were permeabilized using 0.1% Triton X-100 in PBS for 10 min at room temperature. To prevent non-specific binding, the sections were incubated with 10% normal goat serum (cat. no. 16210064; Gibco; Thermo Fisher Scientific, Inc.) in PBS for 1 h at room temperature. The sections were incubated overnight at 4˚C with the following primary antibodies: Anti-LC3 (rabbit polyclonal; cat. no. ab63817; Abcam; 1 μg/ml), anti-p62 (rabbit polyclonal; cat. no. ab155686; Abcam; 1:500), anti-ATG5 (rabbit recombinant monoclonal; cat. no. ab108327; Abcam; 1:100), anti-ABCA1 (mouse

monoclonal; cat. no. ab18180; Abcam; 1:200), and anti-ABCG1 (rabbit polyclonal; cat. no. 13578-1-AP, Proteintech Group, Inc.; 1:200). Following incubation, the sections were washed with PBS and subsequently incubated with horseradish peroxidase (HRP)-conjugated secondary antibodies for 1 h at room temperature. The specific secondary antibodies employed were HRP-conjugated goat anti-rabbit IgG (H+L) (for rabbit primary antibodies; cat. no. 31460; Invitrogen; Thermo Fisher Scientific, Inc.) at a dilution of 1:200, and HRP-conjugated goat anti-mouse IgG (H+L) (for the mouse primary antibody, cat. no. 31430, Invitrogen; Thermo Fisher Scientific, Inc.) also at a dilution of 1:200. Immunoreactivity was visualized employing a 3,3'-diaminobenzidine (DAB) chromogen detection kit (cat. no. GK500705; Gene Tech Biotechnology Co., Ltd.). Image acquisition was performed using an Olympus BX50 (Olympus Corporation) microscope equipped with a digital color camera, and quantitative analysis was conducted using ImageJ software (version 1.8.0; National Institutes of Health).

AAV construction. AAV production and tail vein injection. AAV serotype 9 (AAV9) vectors expressing shRNA targeting FTO (AAV-sh-FTO) or a negative control shRNA (AAV-sh-NC) were packaged in AAV-293 cells using the triple-plasmid transfection system, following the manufacturer's standard protocol (Shanghai GenePharma Co., Ltd.). Briefly, the AAV vector plasmid containing the shRNA sequence (targeting FTO or negative control) under an appropriate promoter, the helper plasmid encoding AAV9 Rep/Cap genes, and the adenovirus helper plasmid were co-transfected into AAV-293 cells using the proprietary transfection reagent RNAi-Mate (GenePharma). At 72 h following transfection, both the cells and supernatant were collected and subjected to three freeze-thaw cycles. Subsequently, the samples were centrifuged at 2,000 rpm (304 x g) for 5 min at 4˚C to eliminate cellular debris. The clarified lysate was then purified and concentrated to obtain AAV vectors. For *in vivo* delivery, mice received a single dose of $3x10^{11}$ vector genomes of the respective AAV9 vectors, diluted in sterile PBS to a final volume of 200 μl, via lateral tail vein injection. The FTO shRNA sequence (5'-3') was: 5'-AAATAGCCGCTGCTTGTGAGA TT-3'.

RT-qPCR. The extraction of total RNA and subsequent RT-qPCR were conducted as follows: Total RNA was isolated from samples utilizing the TRIzol® reagent (cat. no. 15596026; Invitrogen; Thermo Fisher Scientific, Inc.) in accordance with the manufacturer's protocol. The concentration and purity of the extracted RNA were assessed using a NanoDrop 2000 spectrophotometer (Thermo Fisher Scientific, Inc.). Subsequently, 1 μg of total RNA was reverse-transcribed into complementary DNA (cDNA) employing the PrimeScript RT Master Mix Kit (cat. no. RR036A; Takara Biotechnology Co., Ltd.) as per the manufacturer's instructions. qPCR was executed using the SYBR® Green Supermix Kit (cat. no. 1708882, Bio-Rad Laboratories, Inc.) on an Applied Biosystems 7500 Real-Time PCR System (Thermo Fisher Scientific, Inc.). The thermal cycling conditions were as follows: Initial denaturation at 95˚C for 3 min, followed by 40 cycles of 95˚C for 10 sec, 60˚C for 30 sec, and 72˚C for 30 sec. A melting curve analysis was conducted to verify amplification specificity. Relative gene expression levels were determined using the $2^{-\Delta\Delta Cq}$ method (14). RNA extraction, cDNA synthesis, and qPCR were all conducted following the manufacturers' protocols for the TRIzol® Reagent, PrimeScript RT Master Mix Kit, and SYBR® Green Supermix Kit, respectively. The following primers (human) were used: FTO Forward: 5'-CTTCACCAA GGAGACTGCTATTTC-3'; FTO Reverse: 5'-CAAGGTTCC TGTTGAGCACTCTG-3'; GAPDH Forward: 5'-GGTGGT CTCCTCTGACTTCAA-3'; GAPDH Reverse: 5'-GTTGCT GTAGCCAAATTCGTTGT-3'.

Bafilomycin A1. Bafilomycin A1 (cat. no. B1793; MilliporeSigma) and 3-methyladenine (cat. no. 3-MA; M9281; MilliporeSigma) were employed to regulate autophagy in THP-1-derived foam cells. For the Bafilomycin A1 intervention, cells were exposed to 100 nM Bafilomycin A1 for a duration of 3 h at 37˚C. In the case of 3-MA treatment, cells underwent pre-incubation with 1 mM 3-MA for 45 min prior to subsequent stimulation.

Enzyme-linked immunosorbent assay (ELISA). Serum concentrations of MMP-9, myeloperoxidase (MPO), sCD40L, IL-18, and monocyte chemoattractant protein-1 (MCP-1) were quantified utilizing specific ELISA kits: MMP9 ELISA Kit (cat. nos. ab253227 ab246539; Abcam), MPO ELISA Kit (cat. nos. ab155458 and ab119605; Abcam), CD40L ELISA Kit (cat. nos. ab275105 and ab196268; Abcam), IL-18 ELISA Kit (cat. nos. ab216165 and ab215539; Abcam), and MCP-1 ELISA Kit (cat. nos. ab208979 and ab179886; Abcam), in accordance with the manufacturers' protocols. The activity of m6A demethylase was evaluated using the Epigenase m6A Demethylase Activity/Inhibition Assay Kit (Colorimetric; cat. no. P-9013-96; EpigenTek Group Inc.), following the manufacturer's instructions.

Luciferase reporter assay. THP-1 cells were plated in 24-well plates at a density of $0.5\text{-}2x10^5$ cells per well, 24 h prior to transfection. The cells were co-transfected with the pGL3-ATG5 plasmid, which encodes the firefly luciferase reporter, and the pRL-TK plasmid, serving as the Renilla luciferase control vector (E2241; Promega Corporation). Additionally, shRNAs targeting either FTO (5'-GGACTTAAG GAATCCAGAATT-3') or YTHDF1 (5'-GGACATTGGTAC TTGGGATT-3'), as well as negative control shRNAs (5'-TTC TCCGAACGTGTCACGTTT-3'), were employed. These shRNAs were procured from Guangzhou RiboBio Co., Ltd. The transfection process was facilitated using Lipofectamine® 2000 (cat. no. 11668019; Invitrogen; Thermo Fisher Scientific, Inc.). Each well received a total of 500 ng of plasmid DNA and 1.0-2.5 μl of Lipofectamine® 2000, diluted in Opti-MEM® reduced serum medium (Gibco; Thermo Fisher Scientific, Inc.), following the manufacturer's instructions. At 48 h post-transfection, cells were lysed using passive lysis buffer (Promega Corporation). Firefly and Renilla luciferase activities were subsequently measured using the Dual-Luciferase Reporter Assay System (cat. no. E1910; Promega Corporation) on a luminometer. The relative luciferase activity was determined by calculating the ratio of firefly to Renilla luciferase activity, thereby normalizing for transfection efficiency.

Statistical analysis. Statistical analysis was performed using GraphPad Prism (Version 9; Dotmatics). The results were obtained from a minimum of five independent experiments and are expressed as the mean ± standard deviation (SD). The normality of the data distribution was assessed using the Shapiro-Wilk test. For parametric data, analyses were conducted using Student's t-test or one-way analysis of variance (ANOVA), followed by Bonferroni's post hoc test for multiple comparisons. whereas nonparametric data were evaluated using the Mann-Whitney U test or the Kruskal-Wallis test. The quantification of atherosclerotic lesion areas and the percentage of Masson-positive areas within these lesions was performed using ImageJ software (version 2.14.0/1.54f; National Institutes of Health). $P<0.05$ was considered to indicate a statistically significant difference.

Results

FTO inhibits atherosclerotic plaque stability within THP-1 macrophage-derived foam cells. Given that macrophage lipid accumulation critically promotes atherosclerosis, the potential involvement of FTO in this process was investigated. Initial assessments in THP-1-derived macrophages indicated that ox-LDL stimulation markedly reduced both mRNA and protein expression levels of FTO compared to untreated controls (Fig. 1A), implicating FTO in lipid metabolism. Following this association, its functional role was further defined. In THP-1-derived foam cells, FTO expression was manipulated through either overexpression using LV-FTO or knockdown with shRNA-FTO, with LV-Mock and Scr-shRNA serving as controls. Transfection efficiency was confirmed by RT-qPCR analysis (Fig. S1). HPLC analysis demonstrated that FTO overexpression markedly decreased intracellular TC levels, accompanied by reductions in its components, CE and FC. Conversely, FTO knockdown resulted in increased levels of intracellular TC, FC and CE (Fig. 1B and C). These findings indicate that FTO plays a protective role against lipid accumulation in macrophage-derived foam cells.

Reduced cholesterol efflux via ABCA1 and ABCG1 markedly contributes to intracellular lipid accumulation (15). To elucidate the mechanism by which FTO exerts its protective effects, the impact of FTO on the expression of key cholesterol transporters and cholesterol efflux in THP-1 macrophage-derived foam cells was analyzed. FTO overexpression was found to upregulate both mRNA and protein levels of ABCA1 and ABCG1 (Fig. 1D and E). Given that enhanced cholesterol influx mediated by scavenger receptors, such as CD36 and SR-A, also promotes lipid accumulation (16,17), their expression levels were concurrently assessed. Notably, no significant differences in CD36 or SR-A levels were observed following FTO overexpression (Fig. 1F). These results indicate that FTO reduces lipid deposition by specifically promoting ABCA1- and ABCG1-mediated cholesterol export.

In addition to their roles in promoting cholesterol release, ABCA1 and ABCG1 are known to suppress the inflammatory response (18,19). Considering that atherosclerotic plaque stability is negatively associated with inflammatory cell infiltration and necrotic core size, while positively associated with fibrous cap thickness (20), it was hypothesized that FTO might influence plaque stability by modulating inflammation. Supporting this hypothesis, compounds such as the contaminant derivative OXA17 have been shown to stabilize plaques by upregulating ABCA1 (21). Consequently, the effect of FTO on the secretion of pro-inflammatory cytokines and enzymes in THP-1 macrophage-derived foam cells was assessed. FTO knockdown markedly increased the secretion of multiple pro-inflammatory mediators, including MMP-9, MPO, sCD40L), lipoprotein-Associated Phospholipase A2 (Lp-PLA2), IL-18, and MCP-1 (Fig. 1G). These data suggested that FTO mitigates the macrophage inflammatory response, potentially contributing to improved atherosclerotic plaque stability.

FTO promotes autophagy and atherosclerotic plaque stability via upregulating ABCA1 and ABCG1 expression. Autophagy is a multi-step biological process (22). To investigate its regulatory role, functional studies involving both overexpression and knockdown of FTO in THP-1 cells were conducted. Evaluation of key autophagic markers revealed that FTO overexpression elevated the LC3-II/I ratio while decreasing P62 levels (Fig. 2A and B). To directly monitor autophagic flux, the mCherry-EGFP-LC3 reporter system was employed. Consistent with these findings, FTO overexpression increased the number of LC3 puncta. This system distinguishes autophagosomes (yellow puncta, mCherry + EGFP+) from autolysosomes (red puncta, mCherry + EGFP-). Notably, FTO overexpression markedly increased the counts of both yellow and red puncta (Fig. 2C). Furthermore, the addition of BafA1 exacerbated the accumulation of LC3-II induced by FTO knockdown (shRNA-FTO; Fig. 2D). These results indicated that FTO induces autophagy.

To determine whether FTO regulates lipid metabolism and plaque stability through autophagy, autophagic flux in THP-1 macrophage-derived foam cells was modulated using Rapamycin (an agonist) and 3-MA (an inhibitor). Consistent with autophagy-mediated regulation, the upregulation of ABCA1 and ABCG1 expression driven by FTO overexpression was further enhanced by Rapamycin and suppressed by 3-MA (Fig. 2E and F). Similarly, HPLC analysis of intracellular cholesterol revealed that the reduction in TC, FC and CE levels induced by FTO overexpression was markedly amplified by Rapamycin. Conversely, treatment with 3-MA attenuated this effect, leading to increased intracellular accumulation of TC, FC, and CE (Fig. 2G).

These results indicated that FTO alleviates lipid accumulation in THP-1 macrophage-derived foam cells by promoting autophagic flux. Furthermore, the effect of autophagic modulation on the secretion of pro-inflammatory mediators (MMP-9, MPO, sCD40L, Lp-PLA2, IL-18, MCP-1) was assessed. Treatment with the autophagy inhibitor 3-MA increased the levels of these factors, whereas the autophagy inducer Rapamycin markedly reduced their secretion (Fig. 2H). These findings demonstrate that FTO enhances autophagy and promotes atherosclerotic plaque stability by upregulating the expression of ABCA1 and ABCG1.

FTO exerts its influence on autophagy and atherosclerotic plaque stability via m^{6}A-dependent regulation of ATG5. To determine whether FTO regulates m^{6}A modification in THP-1 macrophage-derived foam cells, global m^{6}A levels

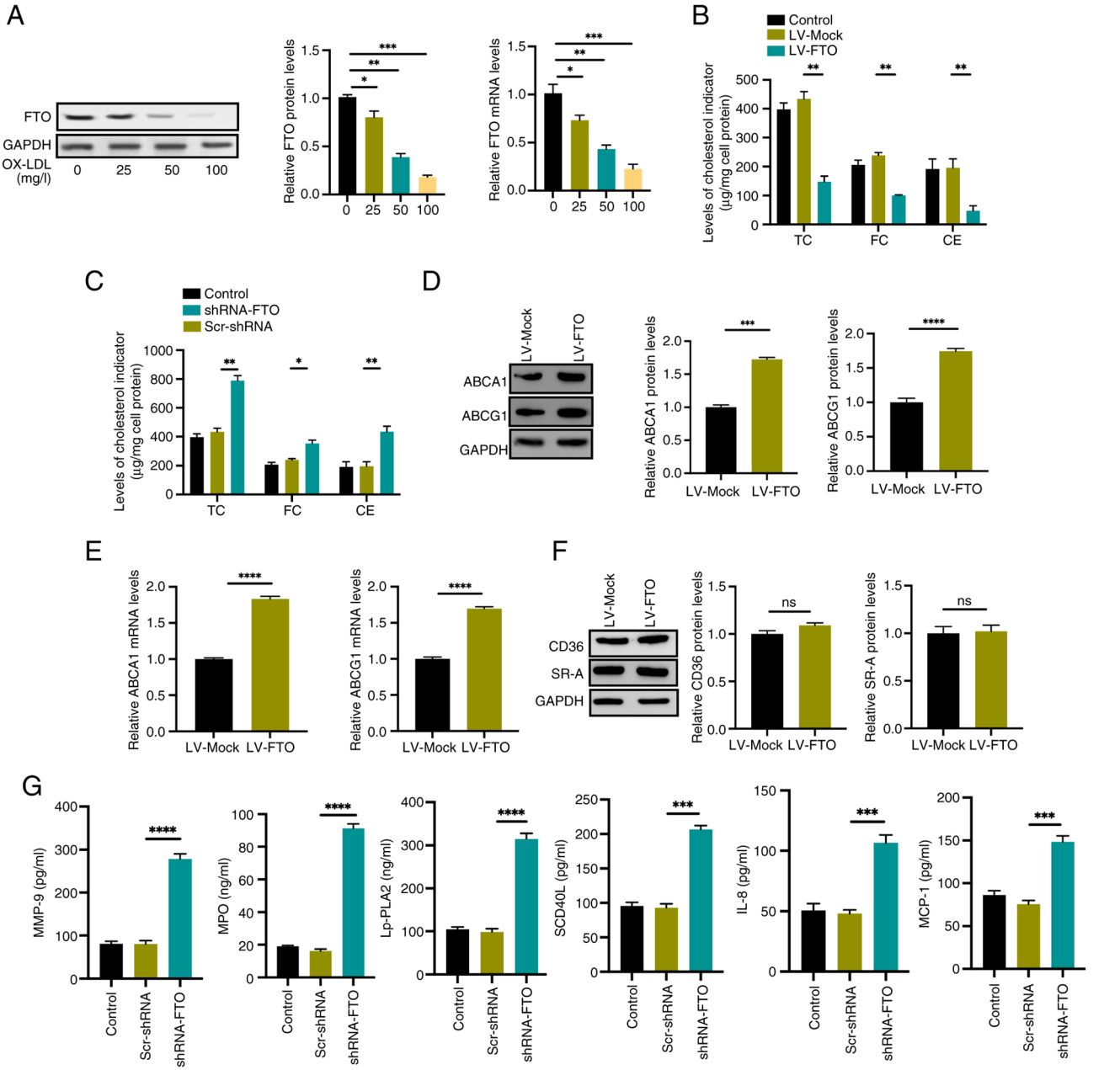

Figure 1. FTO inhibits atherosclerotic plaque stability in THP-1 macrophage-derived foam cells. (A) Analysis of FTO protein and mRNA levels in human THP-1 monocytes treated with increasing concentrations of ox-LDL (0, 25, 50, 100 mg/l) was performed using western blotting and qPCR. (B) Quantification of cellular TC, FC, and CE in THP-1 cells following FTO overexpression was conducted via HPLC. (C) HPLC analysis of TC, FC, and CE levels in THP-1 cells after FTO knockdown. (D and E) Western blotting and qPCR analyses of ABCA1 and ABCG1 protein (D) and mRNA (E) levels upon FTO overexpression or knockdown. (F) Protein levels of CD36 and SR-A were assessed by western blot in response to FTO overexpression. (G) ELISA measurements of MMP-9, MPO, Lp-PLA2, sCD40L, IL-8, and MCP-1 protein levels following FTO knockdown. For all panels, data are derived from n=5 independent experiments; error bars denote standard deviation. *P<0.05, **P<0.01, ***P<0.001, ****P<0.0001. ns, not significant; FTO, fat mass and obesity-associated; qPCR, quantitative PCR; TC, total cholesterol; FC, free cholesterol; CE, cholesteryl ester; HPLC, high performance liquid chromatography; SR-A, scavenger receptor A; ELISA, enzyme-linked immunosorbent assay; MPO, myeloperoxidase; Lp-PLA2, lipoprotein-associated phospholipase A2; sCD40L, soluble CD40 ligand; MCP-1, monocyte chemoattractant protein-1.

were quantified using liquid chromatography-tandem mass spectrometry (LC-MS/MS). FTO knockdown resulted in a significant decrease in m^{6}A modification (Fig. 3A), confirming the role of FTO as an m^{6}A demethylase in these cells. To identify the autophagy-related targets of FTO, several candidate genes were screened via RT-qPCR. The mRNA level of ATG5 was markedly downregulated following FTO knockdown and upregulated upon FTO overexpression (Fig. 3B). Consistent with these findings, FTO overexpression also increased ATG5 protein levels (Fig. 3C). To establish a functional link, a rescue experiment was conducted. Silencing ATG5 effectively reversed the increase in the LC3-II/I ratio and the decrease in SQSTM1/p62 levels induced by FTO overexpression (Fig. 3D), revealing that FTO promotes autophagy primarily by upregulating ATG5 expression.

To assess whether FTO influences lipid accumulation through ATG5, a rescue experiment was again performed. Silencing ATG5 reversed the upregulation of ABCA1 and

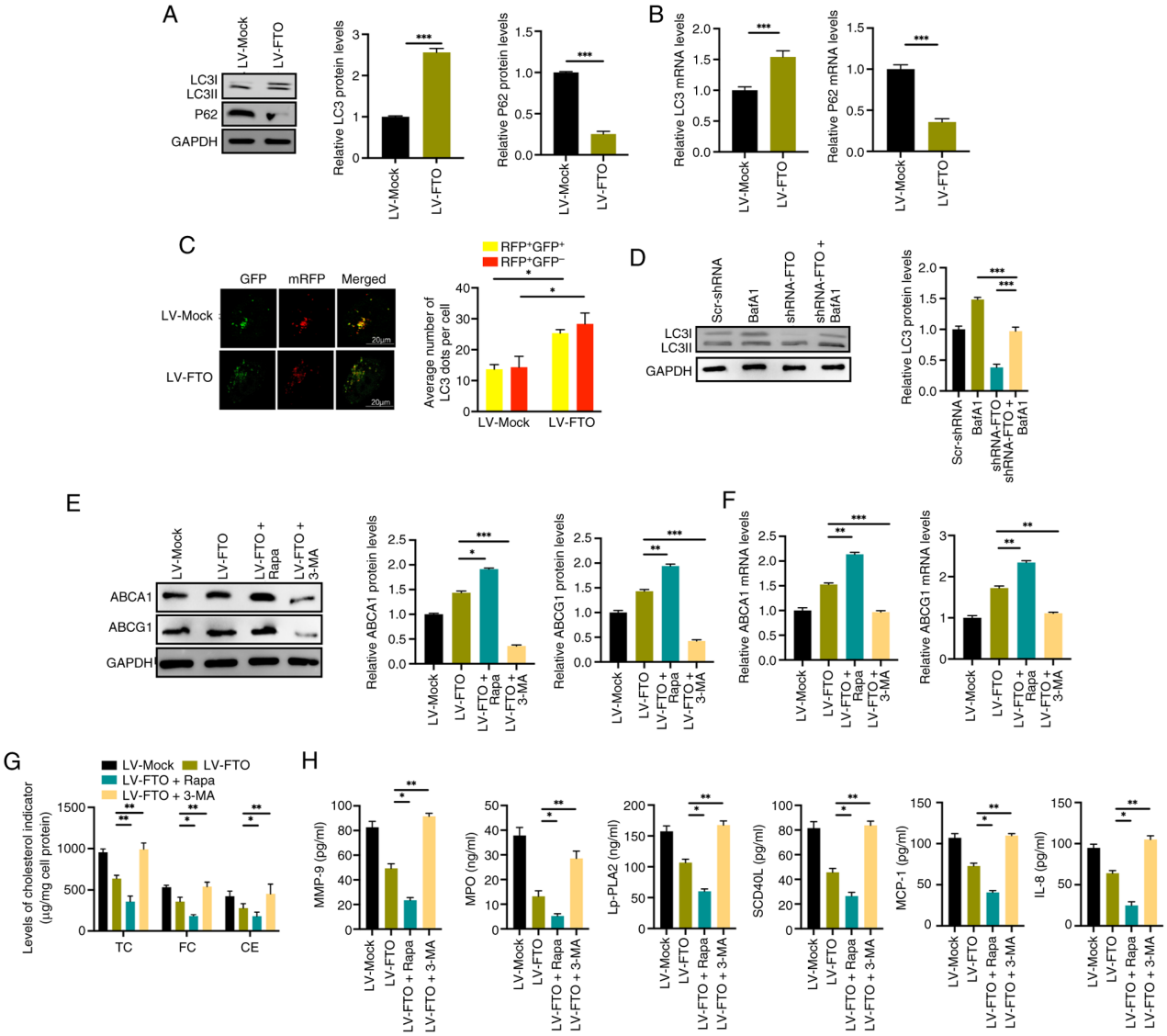

Figure 2. FTO promotes autophagy and atherosclerotic plaque stability via upregulation of ABCA1 and ABCG1 expression. (A) Western blot analysis of protein levels and (B) RT-qPCR analysis of mRNA levels for LC3-II/I and P62 in THP-1 cells following lentiviral FTO overexpression. (C) Autophagic flux was assessed by transfection of the EGFP-mCherry-LC3 reporter into THP-1 cells. Representative images show autophagosomes (yellow) and autolysosomes (red) in control (LV-Mock) and FTO-overexpressing cells, treated with or without Bafilomycin A1 (BafA1; 100 nM, 3 h). Scale bar, 20 μm. (D) Western blot analysis of LC3-II/I protein levels in cells subjected to FTO knockdown, with or without BafA1 co-treatment. Effects of pharmacological modulators (Rapamycin/Rapa, 3-MA) and FTO overexpression on (E) ABCA1 and ABCG1 protein and (F) mRNA expression levels. (G) Cellular cholesterol profiles (TC, FC and CE) measured by HPLC under the indicated conditions of autophagy modulation and FTO overexpression. (H) Secreted levels of inflammatory mediators (MMP-9, MPO, Lp-PLA2, sCD40L, IL-8, MCP-1) quantified by ELISA. Data comprise results from n=5 independent experiments; error bars represent standard deviation. *P<0.05, **P<0.01, ***P<0.001. ns, not significant; FTO, fat mass and obesity-associated; RT-qPCR, reverse transcription-quantitative PCR; ELISA, enzyme-linked immunosorbent assay; TC, total cholesterol; FC, free cholesterol; CE, cholesteryl ester; HPLC, high performance liquid chromatography; MPO, myeloperoxidase; Lp-PLA2, lipoprotein-associated phospholipase A2; sCD40L, soluble CD40 ligand; MCP-1, monocyte chemoattractant protein-1.

ABCG1 induced by FTO overexpression (Fig. 3D and E), indicating that FTO regulates lipid metabolism via ATG5. HPLC analysis confirmed that ATG5 knockdown aggravated the reduction in intracellular TC, FC, and CE levels associated with FTO overexpression (Fig. 3F).

To investigate whether FTO regulates ATG5 through m^{6}A methylation, bioinformatics was initially employed to predict potential m^{6}A modification sites on ATG5 mRNA (Fig. 3G). FTO knockdown decreased the abundance of ATG5 mRNA containing m^{6}A modifications at these sites (Fig. 3H). Methylated RIP-qPCR verified a direct interaction between FTO and ATG5 mRNA in foam cells (Fig. 3I). Furthermore, mRNA stability assays demonstrated that FTO depletion accelerated the decay of ATG5 mRNA transcripts (Fig. 3J). A luciferase reporter assay indicated that FTO knockdown suppressed the activity of a wild-type, but not mutant, ATG5 3' UTR construct (Fig. 3K). Additionally, the data showed that shRNA-ATG5 further upregulated the secretion of pro-inflammatory mediators, including MMP-9, MPO, sCD40L, Lp-PLA2, IL-18, and MCP-1 (Fig. 3L). These data demonstrated that FTO directly targets ATG5 mRNA in an m^{6}A-dependent manner to enhance its stability and expression, thereby promoting autophagy and plaque stability.

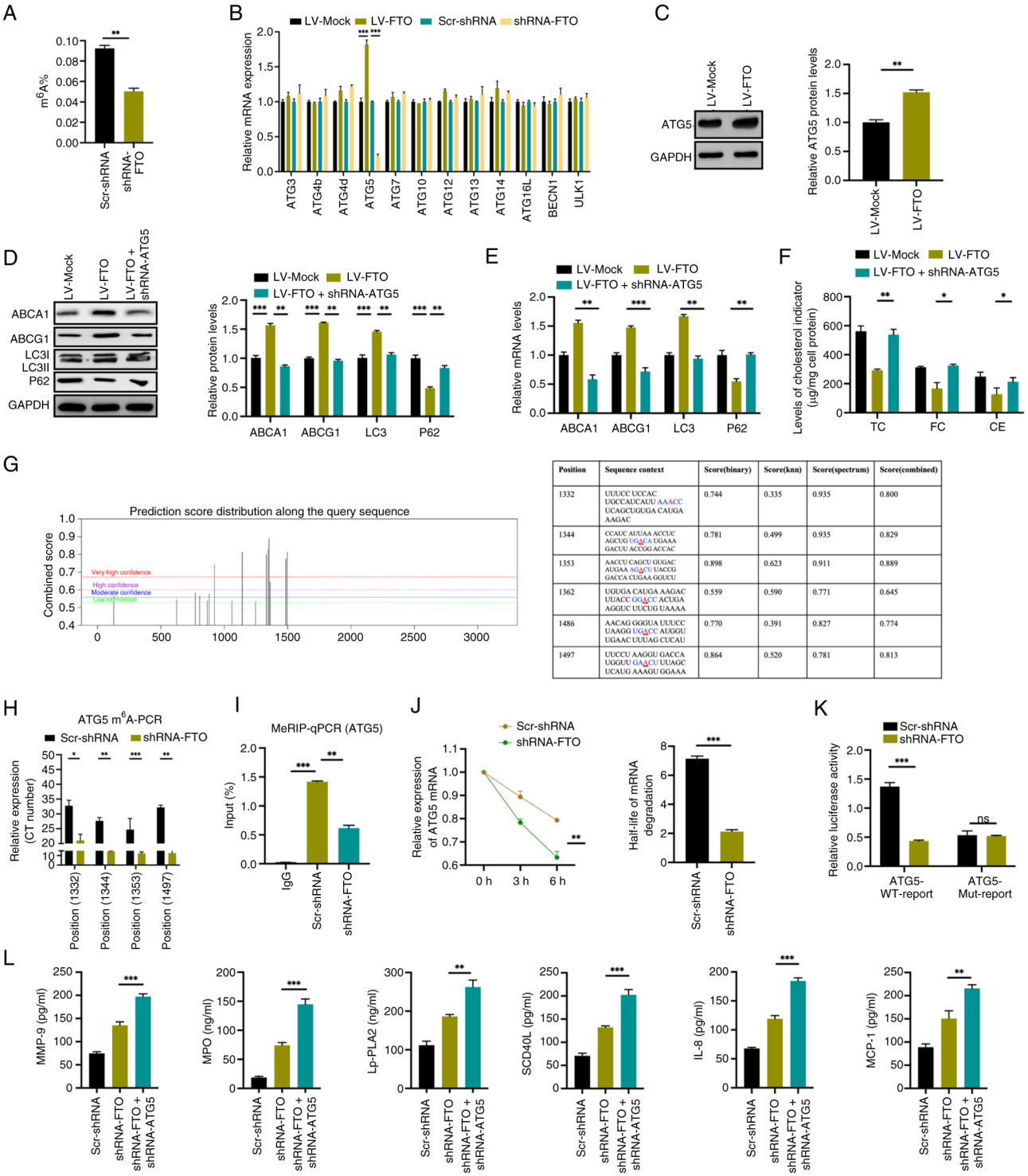

Figure 3. FTO affects autophagy and atherosclerotic plaque stability through targeting ATG5 in an m^{6}A-dependent manner. (A) Global m^{6}A levels in cellular mRNA from control vs. FTO-knockdown cells were quantified using LC-MS/MS. (B) Transcript levels of key ATG genes following FTO overexpression or knockdown were measured by qPCR. (C) ATG5 protein expression in response to FTO overexpression was analyzed by western blotting. (D) Protein and (E) mRNA expression levels of ABCA1, ABCG1, LC3-II/I, and P62 under conditions of combined FTO overexpression and ATG5 knockdown. (F) Cellular cholesterol content (TC, FC and CE) was determined by HPLC in cells subjected to ATG5 knockdown and FTO overexpression. (G) *In silico* prediction of m^{6}A modification sites within ATG5 mRNA was conducted using SRAMP; the conserved RRACH motif is highlighted, with the methylated adenosine underlined. (H) Site-specific quantification of m^{6}A on ATG5 mRNA in control and FTO-deficient cells was performed using the SELECT assay. (I) MeRIP-qPCR analysis demonstrated m^{6}A enrichment on ATG5 mRNA, indicating direct interaction with FTO. (J) ATG5 mRNA stability assay following transcriptional inhibition with Actinomycin D was conducted to calculate the degradation half-life. (K) Luciferase reporter assay comparing the activity of WT and MUT ATG5 3' UTR constructs in control (Scr-shRNA) and FTO-knockdown (shRNA-FTO) cells; firefly luciferase activity was normalized to Renilla luciferase. (L) Secreted levels of inflammatory factors (MMP-9, MPO, Lp-PLA2, sCD40L, IL-8, MCP-1) were quantified by ELISA following ATG5 or FTO knockdown. Data represent n=5 independent experiments. Error bars denote standard deviation. *P<0.05; **P<0.01; ***P<0.001. FTO, fat mass and obesity-associated; ATG, autophagy-related; LC-MS/MS, liquid chromatography-tandem mass spectrometry; HPLC, high-performance liquid chromatography; TC, total cholesterol; FC, free cholesterol; CE, cholesteryl ester; MeRIP-qPCR, m^{6}A RNA immunoprecipitation-quantiative PCR; WT, wild-type; MUT, mutant; sh, short hairpin; MPO, myeloperoxidase; Lp-PLA2, lipoprotein-associated phospholipase A2; sCD40L, soluble CD40 ligand; MCP-1, monocyte chemoattractant protein-1; ELISA, enzyme-linked immunosorbent assay.

YTHDF1 mediates mRNA expression of ATG5 via m^{6}A-dependent mechanism. A previous study established that reader proteins of m^{6}A modification can regulate various aspects of RNA metabolism, including translation, splicing, stability, nuclear export and degradation (23). Among these proteins, the YTH domain-containing family (YTHDF1-3) has been extensively studied. YTHDF2 has been shown to selectively recognize m^{6}A-modified mRNAs and facilitate their decay, while YTHDF1 promotes the translation of m^{6}A-marked transcripts (24,25). YTHDF3 appears to interact with both YTHDF1 and YTHDF2, potentially coordinating their functional roles (26). To determine which YTHDF protein primarily influences ATG5 transcript regulation, individual knockdowns of YTHDF1, YTHDF2 and YTHDF3 were performed using small interfering RNAs, with knockdown efficiency validated for each case (Fig. S2). Knockdown of YTHDF1, but not the other reader proteins, markedly increased ATG5 mRNA levels (Fig. 4A). As depicted in Fig. S3, the knockdown of YTHDF2 via shRNA did not result in a significant alteration of ATG5 or ATG7 protein expression when compared to the Scr-shRNA control. Conversely, shRNA-mediated knockdown of YTHDF1 led to a significant reduction in ATG5 protein levels, while ATG7 levels remained unaffected. Moreover, as illustrated in Fig. S4, the knockdown of FTO did not affect ATG7 at the protein level. This led to the hypothesis that YTHDF1 specifically recognizes FTO-mediated m^{6}A modification on the ATG5 transcript to promote its decay. A rescue experiment supported this notion; YTHDF1 knockdown effectively counteracted the effects of FTO overexpression, restoring the LC3B-II/LC3B-I ratio and ABCA1/ABCG1 expression while reducing P62 accumulation (Fig. 4B and C), thus demonstrating that YTHDF1 is a key mediator in the m^{6}A-dependent regulation of ATG5 by FTO. Furthermore, immunofluorescence analysis using the mCherry-EGFP-LC3 reporter in foam cells revealed that the increase in autophagic puncta (both red and yellow) induced by LV-FTO was further augmented upon treatment with shRNA-YTHDF1 (Fig. 4D).

Additionally, RIP-qPCR experiments confirmed a direct interaction between ATG5 mRNA and YTHDF1 (Fig. 4E). Subsequent mRNA stability assays demonstrated that YTHDF1 knockdown delayed the decay of ATG5 transcripts and enhanced their stability (Fig. 4F). In luciferase reporter assays, FTO knockdown suppressed the activity of wild-type constructs but had no effect on mutant constructs (Fig. 4G). HPLC analysis indicated that YTHDF1 knockdown reversed the cholesterol-lowering effect of FTO overexpression, as evidenced by restored intracellular levels of TC, FC and CE (Fig. 4H). Furthermore, in a rescue experiment, YTHDF1 knockdown counteracted the changes in the secretion of MMP-9, MPO, sCD40L, Lp-PLA2, IL-18 and MCP-1 induced by FTO overexpression (Fig. 4I). In summary, these results revealed that YTHDF1 regulates ATG5 mRNA expression via an m^{6}A-dependent mechanism.

FTO regulates plaque stability through ATG5-dependent autophagy in vivo. To further elucidate the relationship between FTO and atherosclerotic plaque composition, plaque size in aortic tissues was evaluated using hematoxylin-eosin staining, while collagen content was assessed via Masson's trichrome staining. Hematoxylin-eosin staining revealed that atherosclerotic lesions in AAV-sh-FTO-treated mice were larger, exhibited increased lipid accumulation, and demonstrated thicker fibrous caps compared to controls. Masson's staining further indicated a significant reduction in collagen fiber content within plaques from AAV-sh-FTO mice relative to the AAV-Mock group (Fig. 5A). Immunofluorescence co-localization analysis on arterial plaque sections was performed to determine the cellular localization of FTO in endothelial cells (CD31$^+$), smooth muscle cells (αSMA$^+$) and macrophages (CD68$^+$). The results demonstrated that FTO predominantly localizes within macrophages (Fig. 5B). Immunohistochemical analysis of key autophagy and cholesterol efflux-related proteins showed that levels of LC3, ATG5, ABCA1 and ABCG1 were downregulated, while P62 expression was upregulated in the AAV-sh-FTO group (Fig. 5C). Moreover, the production of plaque destabilization markers-including MMP-9, MPO, sCD40L, Lp-PLA2, IL-18 and MCP-1 was markedly upregulated in AAV-sh-FTO mice (Fig. 5D). These findings indicate that FTO knockdown exacerbates atherosclerotic plaque development and instability, likely due to impaired autophagic flux and cholesterol homeostasis, accompanied by enhanced inflammation. In conclusion, these findings support a protective role for FTO in mitigating the progression of atherosclerosis.

Discussion

Atherosclerotic cardiovascular disease (ASCVD) continues to be a leading cause of mortality worldwide, highlighting the inadequacies of existing therapeutic approaches in effectively reducing its effects (27,28). The progression to acute and often fatal coronary events is commonly triggered by the rupture of unstable atherosclerotic plaques (29). Consequently, understanding the molecular pathways that regulate plaque stability is a crucial research priority. Investigating these mechanisms is vital for the development of complementary diagnostic strategies and interventions designed to prevent disease progression and avert acute cardiovascular events.

Autophagy is a conserved catabolic process crucial for maintaining cellular homeostasis, characterized by the degradation of damaged cytoplasmic components within lysosomes. This dynamic process begins with the conversion of LC3-I to the lipidated LC3-II form, a hallmark of autophagosome formation (30), and concludes with lysosomal degradation. In advanced atherosclerosis, this process is often dysregulated (31,32), leading to exacerbated plaque pathogenesis through the promotion of vascular aging and cellular dysfunction. Notably, the genetic ablation of core autophagy components, such as ATG5, increases apoptosis and oxidative stress, thereby contributing to plaque necrosis (33). The present study identified FTO as a significant factor within this critical pathway. It demonstrated that FTO overexpression enhances autophagic flux, with experiments involving Bafilomycin A1 suggesting that this effect is primarily mediated through the promotion of autophagosome synthesis. This significant connection between FTO-driven m^{6}A demethylation and the enhancement of autophagy highlights the therapeutic potential of targeting this axis to stabilize atherosclerotic plaques.

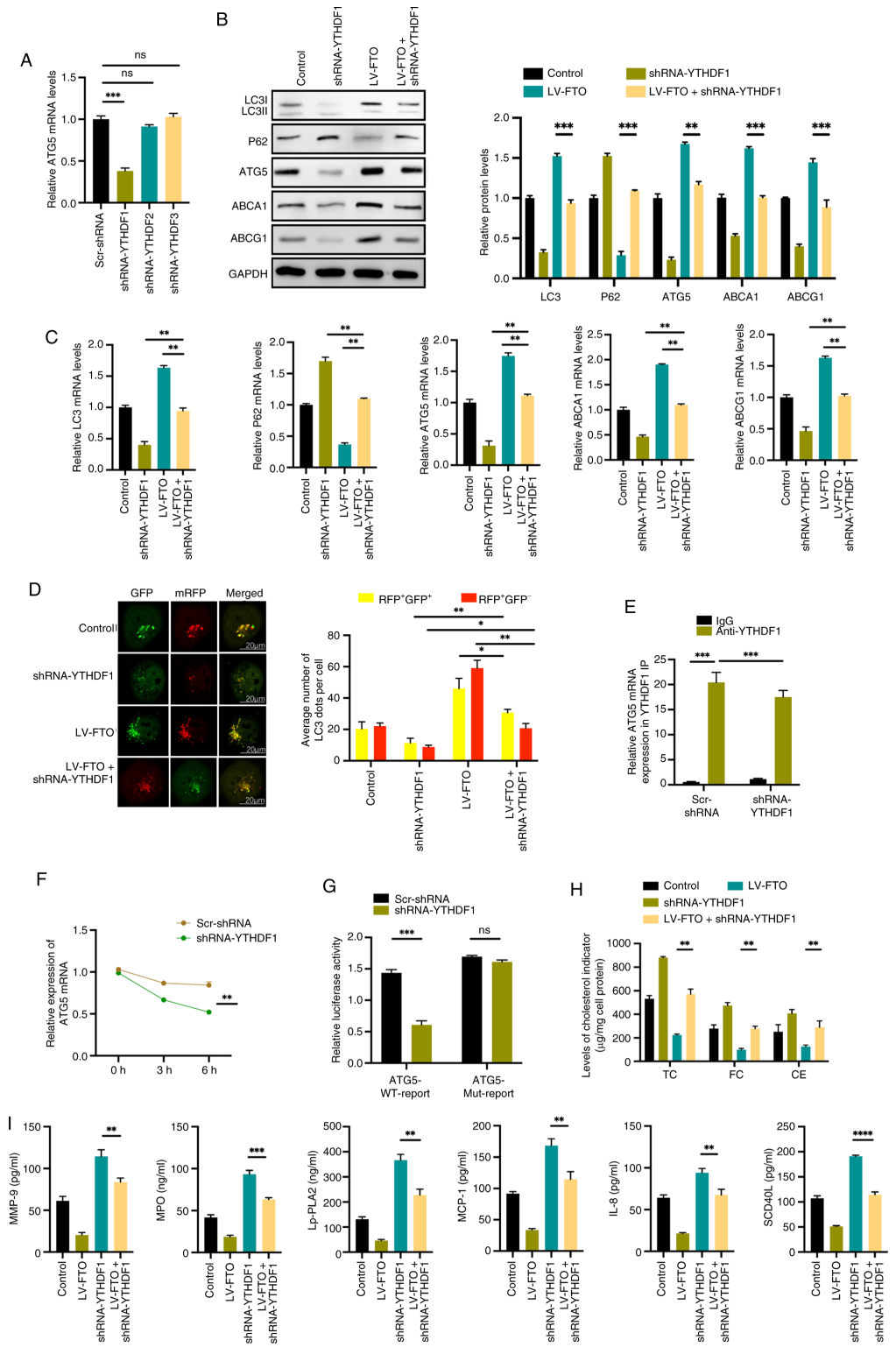

Figure 4. YTHDF1 mediates mRNA expression of ATG5 through an m^{6}A-dependent mechanism. (A) ATG5 mRNA levels in THP-1 cells following individual knockdown of YTHDF1, YTHDF2, or YTHDF3 were analyzed by qPCR. (B) Protein and (C) mRNA expression levels of LC3-II/I, P62, ATG5, ABCA1, and ABCG1 in cells subjected to FTO overexpression or YTHDF1 knockdown. (D) Autophagic flux was assessed by imaging of EGFP-mCherry-LC3 puncta (autophagosomes, yellow; autolysosomes, red) in YTHDF1 knockdown and FTO overexpressing cells. Scale bar, 20 μm. (E) RIP-qPCR analysis of the interaction between YTHDF1 and ATG5 mRNA in control vs. YTHDF1-knockdown cells, with enrichment normalized to input. (F) ATG5 mRNA stability assay conducted following transcriptional inhibition with Actinomycin D; degradation half-life is shown. (G) Relative luciferase activity of WT vs. MUT ATG5 3' UTR reporter constructs in cells transfected with control (Scr-shRNA) or YTHDF1-targeting (shRNA-YTHDF1) vectors; firefly luciferase activity was normalized to *Renilla* luciferase activity. (H) Cellular cholesterol content (TC, FC and CE) quantified by HPLC in response to YTHDF1 knockdown and FTO overexpression. (I) Secreted levels of inflammatory mediators (MMP-9, MPO, Lp-PLA2, sCD40L, IL-8, MCP-1) were measured by ELISA following YTHDF1 knockdown or FTO overexpression. Data are representative of n=5 independent experiments. Error bars denote standard deviation. *P<0.05; **P<0.01; ***P<0.001; ****P<0.001. ns, not significant. YTHDF, YTH domain-containing family; qPCR, quantitative PCR; FTO, fat mass and obesity-associated; RIP-qPCR, RNA immunoprecipitation-quantitative PCR; WT, wild-type; MUT, mutant; sh, short hairpin; TC, total cholesterol; FC, free cholesterol; CE, cholesteryl ester; MPO, myeloperoxidase; Lp-PLA2, lipoprotein-associated phospholipase A2; sCD40L, soluble CD40 ligand; MCP-1, monocyte chemoattractant protein-1.

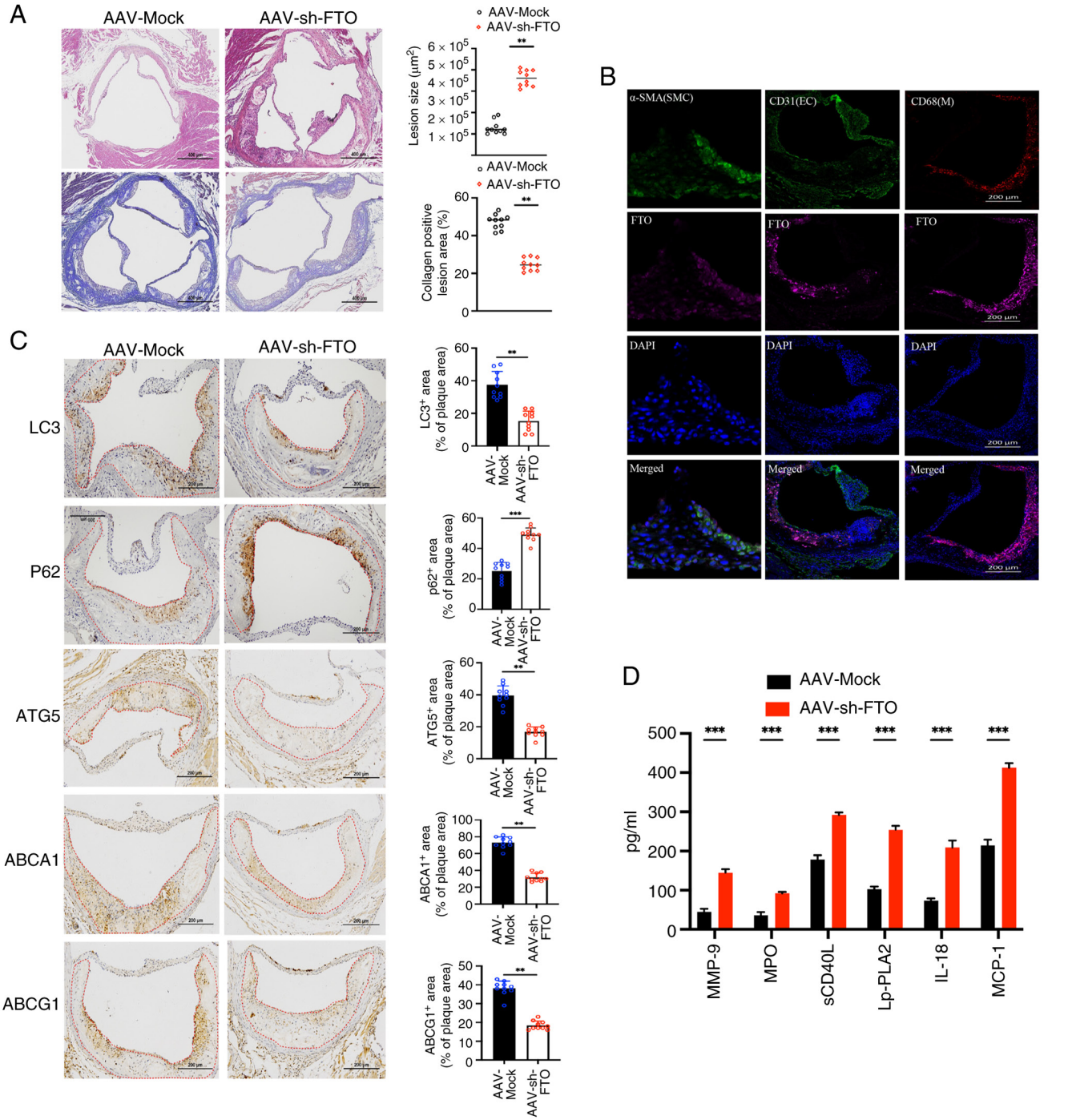

Figure 5. FTO regulates plaque stability through ATG5-dependent autophagy *in vivo*. (A) Representative hematoxylin-eosin staining images and Masson's trichrome staining of aortic valve sections, comparing atherosclerotic lesion areas between AAV-Mock and AAV-sh-FTO groups fed with HFD. Data are derived from n=10 independent experiments. **P<0.01. Magnification, x100. (B) FTO cellular localization in plaques was demonstrated by co-staining with CD31 (endothelium), CD68 (macrophages) and α-SMA (smooth muscle cells). Magnification, x200. n=10 independent experiments. (C) Immunohistochemical detection of LC3, P62, ATG5, ABCA1, and ABCG1 in aortic valves. Quantification of LC3, P62, ATG5, ABCA1, and ABCG1 areas is shown. n=10 independent experiments. **P<0.01; ***P<0.001. Magnification, x200. (D) ELISA quantification of MMP-9, MPO, SCD40L, Lp-PLA2, IL-18, and MCP-1 chemokines normalized to tissue protein content. n=10 independent experiments. ***P<0.001. FTO, fat mass and obesity-associated; sh, short hairpin; HFD, high-fat diet; ELISA, enzyme-linked immunosorbent assay; MPO, myeloperoxidase; Lp-PLA2, lipoprotein-associated phospholipase A2; sCD40L, soluble CD40 ligand; MCP-1, monocyte chemoattractant protein-1; α-SMA, α-smooth muscle actin.

Autophagy, a conserved intracellular degradative mechanism, is pivotal in the renewal and recycling of cellular components to maintain nutrient and energy homeostasis within the cell. ATG5, a critical element of the autophagy process, is instrumental in the formation of the autophagosome, a defining feature of autophagy. ATG5 interacts with ATG12 and ATG16L1 to form an E3-like ligase complex, which is essential for autophagosome expansion. This process is meticulously regulated, with autophagy-related (ATG) proteins playing key roles. Among the 41 identified ATG genes, ATG5 is indispensable for autophagosome formation and positively influences autophagic activity (34). Moreover,

m6A-modified USP13 has been shown to induce autophagy and imatinib resistance in gastrointestinal stromal tumor cells by modulating ATG5 stability. The present study indicated that FTO regulates ATG5 mRNA expression in an m6A-dependent manner, thereby affecting autophagy. A similar mechanism was observed in a recent study, where FTO was found to coordinate autophagy and energy metabolism by regulating ATG16L1 in an m6A-dependent manner in osteoarthritis (35). FTO acts as a catalyst for diabetic wound healing and influences autophagy by regulating TRIB3 in keratinocytes (36). This variation may be attributed to the specificity of m6A methylation in autophagy across different tissue or cell types. mRNA transcripts modified with m6A display distinct terminal structures due to recognition by various m6A-binding proteins. YTHDF2 and YTHDF3 work synergistically to promote the degradation of target mRNA, thereby decreasing target gene expression. By contrast, YTHDF1 and YTHDF3 collaborate to enhance the translation of target mRNA, thus increasing target gene expression (37,38). IGF2BPs contribute to mRNA stability, thereby augmenting translational efficiency (39). The findings suggested that YTHDF1 mediates the stability of ATG5 mRNA in an m6A-dependent manner, identifying ATG5 mRNA as a target gene of YTHDF1.

In recent years, there has been an increasing scholarly focus on the role of FTO-mediated m^6A RNA methylation in the context of cardiovascular disease. Genome-wide association studies have definitively associated genetic variants within the FTO gene with an elevated risk of several cardiovascular conditions, such as hypertension, myocardial infarction, acute coronary syndrome and graft rejection in heart transplant recipients (40-44). Nonetheless, the direct functions and specific molecular mechanisms by which FTO influences the fundamental pathophysiology of atherosclerosis are not yet fully elucidated.

Emerging evidence indicates that FTO plays complex, cell-type-specific roles in atherosclerosis. For example, in endothelial cells, FTO overexpression has been shown to diminish the protective effects of Rb1 against atherosclerotic pathologies and VCAM-1 expression in $Apoe^{-/-}$ mice (45). Conversely, in vascular smooth muscle cells (VSMCs), FTO appears to mitigate ox-LDL-induced senescence, thereby inhibiting VSMC aging within plaques (46). While these studies underscore protective roles in specific cellular contexts, a fundamental question persists: Does FTO regulate atherosclerosis through a unifying, cross-cellular mechanism? Additionally, the potential direct influence of FTO on critical plaque biology, such as autophagy, via m^6A demethylation remains entirely unexplored.

The present study endeavored to fill this significant knowledge gap by elucidating the role of autophagy as a pivotal downstream pathway through which FTO influences atherosclerosis. It provided novel evidence demonstrating that FTO directly targets the mRNA of ATG5, a critical gene involved in autophagy, in a manner dependent on m^6A modification. This interaction enhances the stability of ATG5 mRNA and its protein expression, thereby facilitating autophagic flux. This discovery aligns with the broader emerging paradigm that recognizes m^6A modification as an essential upstream regulator of autophagy (47,48). This study represents the first documentation of the direct demethylation of ATG5 mRNA by the enzyme FTO, commonly referred to as the 'eraser', specifically within the context of atherosclerosis. This finding highlighted the mechanistic specificity of the present study. Furthermore, the present study demonstrated the pathophysiological significance of this axis through a comprehensive series of *in vitro* and *in vivo* experiments. Its results provided robust evidence that the FTO-ATG5-autophagy signaling axis enhances plaque stability. The present study introduced a novel paradigm for understanding RNA epitranscriptomics in cardiovascular disease, where m^6A-dependent regulation of autophagy directly impacts disease progression and plaque phenotype.

Traditionally, YTHDF1 has been acknowledged as a promoter of translation; however, recent research indicates that it can also facilitate mRNA degradation in a context-dependent manner (49,50). Notably, the knockdown of YTHDF2 does not influence the expression of ATG5 or ATG7 in macrophages stimulated with ox-LDL, whereas the depletion of YTHDF1 results in decreased ATG5 levels. Furthermore, FTO does not regulate ATG7 in our experimental model. Although Wang *et al* (51) reported that YTHDF2 mediates the m^6A-dependent degradation of Atg5 and Atg7 in adipocytes and hepatocytes, the functional roles of m^6A readers are increasingly understood to be context-dependent (52). Studies have challenged the traditional YTHDF model, revealing that all three paralogs redundantly mediate mRNA degradation. YTHDF1 facilitates decay through CCR4-NOT and AGO2-mediated phase separation, underscoring its context-dependent role in mRNA stability (49,50,53). Consequently, the identification of YTHDF1 as the principal m^6A reader regulating ATG5 in macrophages is consistent with contemporary models of m^6A regulation.

Several limitations warrant acknowledgment. First, the findings were exclusively based on $ApoE^{-/-}$ mouse models and *in vitro* macrophage lines, lacking validation in human plaques. This limitation restricts the direct translational relevance of the FTO-ATG5-YTHDF1 axis to patient scenarios. To address this, future research will analyze human carotid endarterectomy samples (comparing stable and symptomatic plaques) for expression levels of FTO, ATG5 and YTHDF1, as well as their correlation with plaque stability. Second, unbiased MeRIP-seq in FTO-knockdown macrophages will help identify additional autophagy-related targets of FTO. Third, techniques such as RNA pull-down, CLIP-seq and macrophage-specific FTO knockout mice will be employed to dissect the precise molecular mechanisms underlying YTHDF1-mediated ATG5 mRNA degradation. Addressing these limitations will enhance the translational potential of this epitranscriptomic axis, although this potential requires validation through future clinical studies.

Acknowledgements

Not applicable.

Funding

The present study was supported by The Key Project of Medical Science and Technology of Henan Province (grant no. LHGJ20230009), and Science and Technology Tackling in Henan Province (grant no. 232102310084).

Availability of data and materials

The data generated in the present study may be requested from the corresponding author.

Authors' contributions

FG and KZ was responsible for conceptualization, data curation, formal analysis, methodology, project administration, supervision, validation, visualization, writing the original draft, reviewing and editing. BH was responsible for data curation, formal analysis, methodology and validation. FG and KZ were responsible for data curation and formal analysis. YL designed the study. FG and BH confirm the authenticity of all the raw data. MH was responsible for conducting the animal experiments, managing the ethics approval process, and revising the sections on animal experiment methods and ethical statements within the manuscript. All authors read and approved the final manuscript.

Ethics approval and consent to participate

All procedures adhered to the NIH guidelines (Publication No. 85-23, 1996 revision) and received approval from the Animal Ethics Committee of Zhengzhou No. 7 People's Hospital (approval no. 2024-017).

Patient consent for publication

Not applicable.

Competing interests

The authors declare that they have no competing interests.

References

1. Cagnina A, Chabot O, Davin L, Lempereur M, Maréchal P, Oury C and Lancellotti P: Atherosclerosis, an inflammatory disease. Rev Med Liege 77: 302-309, 2022 (In French).
2. Wolf D and Ley K: Immunity and inflammation in atherosclerosis. Circ Res 124: 315-327, 2019.
3. Libby P: Molecular bases of the acute coronary syndromes. Circulation 91: 2844-2850, 1995.
4. Dong G, Yu J, Shan G, Su L, Yu N and Yang S: N6-methyladenosine methyltransferase METTL3 promotes angiogenesis and atherosclerosis by upregulating the JAK2/STAT3 pathway via m6A reader IGF2BP1. Front Cell Dev Biol 9: 731810, 2021.
5. Wing MR, Ziegler J, Langefeld CD, Ng MC, Haffner SM, Norris JM, Goodarzi MO and Bowden DW: Analysis of FTO gene variants with measures of obesity and glucose homeostasis in the IRAS family study. Hum Genet 125: 615-626, 2009.
6. Jalili V, Mokhtari Z, Rastgoo S, Hajipour A, Bourbour F, Gholamalizadeh M, Mosavi Jarrahi A, JavadiKooshesh S, Moslem A, Abdollahi M and Doaei S: The association between FTO rs9939609 polymorphism and serum lipid profile in adult women. Diabetol Metab Syndr 13: 138, 2021.
7. Levine B and Kroemer G: Biological functions of autophagy genes: A disease perspective. Cell 176: 11-42, 2019.
8. Mizushima N and Levine B: Autophagy in human diseases. N Engl J Med 383: 1564-1576, 2020.
9. Leidal AM, Levine B and Debnath J: Autophagy and the cell biology of age-related disease. Nat Cell Biol 20: 1338-1348, 2018.
10. Gulati P, Cheung MK, Antrobus R, Church CD, Harding HP, Tung YC, Rimmington D, Ma M, Ron D, Lehner PJ, *et al*: Role for the obesity-related FTO gene in the cellular sensing of amino acids. Proc Natl Acad Sci USA 110: 2557-2562, 2013.
11. Aas A, Isakson P, Bindesboll C, Alemu EA, Klungland A and Simonsen A: Nucleocytoplasmic shuttling of FTO does not affect starvation-induced autophagy. PLoS One 12: e0168182, 2017.
12. Jin S, Zhang X, Miao Y, Liang P, Zhu K, She Y, Wu Y, Liu DA, Huang J, Ren J and Cui J: m^6A RNA modification controls autophagy through upregulating ULK1 protein abundance. Cell Res 28: 955-957, 2018.
13. Dong XH, Lu ZF, Kang CM, Li XH, Haworth KE, Ma X, Lu JB, Liu XH, Fang FC, Wang CS, *et al*: The long noncoding RNA RP11-728F11.4 promotes atherosclerosis. Arterioscler Thromb Vasc Biol 41: 1191-1204, 2021.
14. Livak KJ and Schmittgen TD: Analysis of relative gene expression data using real-time quantitative PCR and the 2(-Delta Delta C(T)) method. Methods 25: 402-408, 2001.
15. Rawlins SC: Biological control of insect pests affecting man and animals in the tropics. Crit Rev Microbiol 16: 235-252, 1989.
16. Kunjathoor VV, Febbraio M, Podrez EA, Moore KJ, Andersson L, Koehn S, Rhee JS, Silverstein R, Hoff HF and Freeman MW: Scavenger receptors class A-I/II and CD36 are the principal receptors responsible for the uptake of modified low density lipoprotein leading to lipid loading in macrophages. J Biol Chem 277: 49982-49988, 2002.
17. Bhargava P, Dinh D, Teramayi F, Silberg A, Petler N, Anderson AM, Sadrerafi K, Clemens DM and O'Connor MS: Selective removal of 7KC by a novel atherosclerosis therapeutic candidate reverts foam cells to a macrophage-like phenotype. bioRxiv [Preprint]: 2023.10.23.563623, 2023.
18. Yin K, Liao DF and Tang CK: ATP-binding membrane cassette transporter A1 (ABCA1): A possible link between inflammation and reverse cholesterol transport. Mol Med 16: 438-449, 2010.
19. Wojcik AJ, Skaflen MD, Srinivasan S and Hedrick CC: A critical role for ABCG1 in macrophage inflammation and lung homeostasis. J Immunol 180: 4273-4282, 2008.
20. Vakili H, Shirazi M, Charkhkar M, Khaheshi I, Memaryan M and Naderian M: Correlation of platelet-to-lymphocyte ratio and neutrophil-to-lymphocyte ratio with thrombolysis in myocardial infarction frame count in ST-segment elevation myocardial infarction. Eur J Clin Invest 47: 322-327, 2017.
21. Tsui PF, Chern CY, Lien CF, Lin FY, Tsai CS, Tsai MC and Lin CS: An octimibate derivative, Oxa17, enhances cholesterol efflux and exerts anti-inflammatory and atheroprotective effects in experimental atherosclerosis. Biochem Pharmacol 188: 114581, 2021.
22. Li R, Wei X and Jiang DS: Protein methylation functions as the posttranslational modification switch to regulate autophagy. Cell Mol Life Sci 76: 3711-3722, 2019.
23. Song D, Hou J, Wu J and Wang J: Role of N^6-methyladenosine RNA modification in cardiovascular disease. Front Cardiovasc Med 8: 659628, 2021.
24. Wang X, Zhao BS, Roundtree IA, Lu Z, Han D, Ma H, Weng X, Chen K, Shi H and He C: N(6)-methyladenosine modulates messenger RNA translation efficiency. Cell 161: 1388-1399, 2015.
25. Du H, Zhao Y, He J, Zhang Y, Xi H, Liu M, Ma J and Wu L: YTHDF2 destabilizes m(6)A-containing RNA through direct recruitment of the CCR4-NOT deadenylase complex. Nat Commun 7: 12626, 2016.
26. Roost C, Lynch SR, Batista PJ, Qu K, Chang HY and Kool ET: Structure and thermodynamics of N6-methyladenosine in RNA: A spring-loaded base modification. J Am Chem Soc 137: 2107-2115, 2015.
27. Yvan-Charvet L, Bonacina F, Guinamard RR and Norata GD: Immunometabolic function of cholesterol in cardiovascular disease and beyond. Cardiovasc Res 115: 1393-1407, 2019.
28. Yu XH, Zheng XL and Tang CK: Peroxisome proliferator-activated receptor α in lipid metabolism and atherosclerosis. Adv Clin Chem 71: 171-203, 2015.
29. Petkovic A, Erceg S, Munjas J, Ninic A, Vladimirov S, Davidovic A, Vukmirovic L, Milanov M, Cvijanovic D, Mitic T and Sopic M: LncRNAs as regulators of atherosclerotic plaque stability. Cells 12: 1832, 2023.
30. Kabeya Y, Mizushima N, Ueno T, Yamamoto A, Kirisako T, Noda T, Kominami E, Ohsumi Y and Yoshimori T: LC3, a mammalian homologue of yeast Apg8p, is localized in autophagosome membranes after processing. EMBO J 19: 5720-5728, 2000.
31. Vion AC, Kheloufi M, Hammoutene A, Poisson J, Lasselin J, Devue C, Pic I, Dupont N, Busse J, Stark K, *et al*: Autophagy is required for endothelial cell alignment and atheroprotection under physiological blood flow. Proc Natl Acad Sci USA 114: E8675-E8684, 2017.

32. LaRocca TJ, Henson GD, Thorburn A, Sindler AL, Pierce GL and Seals DR: Translational evidence that impaired autophagy contributes to arterial ageing. J Physiol 590: 3305-3316, 2012.
33. Liao X, Sluimer JC, Wang Y, Subramanian M, Brown K, Pattison JS, Robbins J, Martinez J and Tabas I: Macrophage autophagy plays a protective role in advanced atherosclerosis. Cell Metab 15: 545-553, 2012.
34. Changotra H, Kaur S, Yadav SS, Gupta GL, Parkash J and Duseja A: ATG5: A central autophagy regulator implicated in various human diseases. Cell Biochem Funct 40: 650-667, 2022.
35. Jiang Z, Zhang C, Liu R, Zhu Z, Long D, Wen X, Yang Z, Jiang D, Mao G, Liao W and Zhang Z: M^6A demethyltransferase FTO attenuates meniscus degeneration and osteoarthritis via orchestrating autophagy and energetic metabolism. Adv Sci (Weinh) 12: e2412379, 2025.
36. Dong Z, Li S, Huang Y, Chen T, Ding Y and Tan Q: RNA N^6-methyladenosine demethylase FTO promotes diabetic wound healing through TRIB3-mediated autophagy in an m^6A-YTHDF2-dependent manner. Cell Death Dis 16: 222, 2025.
37. Liu T, Wei Q, Jin J, Luo Q, Liu Y, Yang Y, Cheng C, Li L, Pi J, Si Y, *et al*: The m6A reader YTHDF1 promotes ovarian cancer progression via augmenting EIF3C translation. Nucleic Acids Res 48: 3816-3831, 2020.
38. Zhang Y, Wang X, Zhang X, Wang J, Ma Y, Zhang L and Cao X: RNA-binding protein YTHDF3 suppresses interferon-dependent antiviral responses by promoting FOXO3 translation. Proc Natl Acad Sci USA 116: 976-981, 2019.
39. Huang H, Weng H, Sun W, Qin X, Shi H, Wu H, Zhao BS, Mesquita A, Liu C, Yuan CL, *et al*: Recognition of RNA N^6-methyladenosine by IGF2BP proteins enhances mRNA stability and translation. Nat Cell Biol 20: 285-295, 2018.
40. Ahmad T, Chasman DI, Mora S, Paré G, Cook NR, Buring JE, Ridker PM and Lee IM: The fat-mass and obesity-associated (FTO) gene, physical activity, and risk of incident cardiovascular events in white women. Am Heart J 160: 1163-1169, 2010.
41. He D, Fu M, Miao S, Hotta K, Chandak GR and Xi B: FTO gene variant and risk of hypertension: A meta-analysis of 57,464 hypertensive cases and 41,256 controls. Metabolism 63: 633-639, 2014.
42. Liu C, Mou S and Pan C: The FTO gene rs9939609 polymorphism predicts risk of cardiovascular disease: A systematic review and meta-analysis. PLoS One 8: e71901, 2013.
43. Hubacek JA, Vrablik M, Dlouha D, Stanek V, Gebauerova M, Adamkova V, Ceska R, Dostálová G, Linhart A, Vitek L and Pitha J: Gene variants at FTO, 9p21, and 2q36.3 are age-independently associated with myocardial infarction in Czech men. Clin Chim Acta 454: 119-123, 2016.
44. Hubacek JA, Vymetalova J, Lanska V and Dlouha D: The fat mass and obesity related gene polymorphism influences the risk of rejection in heart transplant patients. Clin Transplant 32: e13443, 2018.
45. Yang Z, Xiong M, Tang X, Wang P, Cui J, Chen Y and Zhang T: Ginsenoside Rb1 mitigates atherosclerosis in part through modulating FTO-mediated m^6A RNA modification in NETs-induced endothelial activation. Front Pharmacol 16: 1631076, 2025.
46. Sun J, Wang M, Jia F, Song J, Ren J and Hu B: FTO stabilizes MIS12 to inhibit vascular smooth muscle cell senescence in atherosclerotic plaque. J Inflamm Res 17: 1857-1871, 2024.
47. Yu H, Zhuang J, Zhou Z, Song Q, Lv J, Yang X, Yang H and Lu Q: METTL16 suppressed the proliferation and cisplatin-chemoresistance of bladder cancer by degrading PMEPA1 mRNA in a m6A manner through autophagy pathway. Int J Biol Sci 20: 1471-1491, 2024.
48. Zhang P, Feng K, Yu X, Yang Y, Luo S, Li Q, Zhang H, Jia Y, Fei Q, Ren X, *et al*: The m6A methyltransferase METTL14 promotes oncogenic Kras induced juvenile myelomonocytic leukemia through dysregulating autophagy. Cell Death Differ 33: 156-170, 2026.
49. Zaccara S and Jaffrey SR: A unified model for the function of YTHDF proteins in regulating m^6A-modified mRNA. Cell 181: 1582-1595.e18, 2020.
50. Zaccara S and Jaffrey SR: Understanding the redundant functions of the m^6A-binding YTHDF proteins. RNA 30: 468-481, 2024.
51. Wang X, Wu R, Liu Y, Zhao Y, Bi Z, Yao Y, Liu Q, Shi H, Wang F and Wang Y: m^6A mRNA methylation controls autophagy and adipogenesis by targeting Atg5 and Atg7. Autophagy 16: 1221-1235, 2020.
52. Shi H, Wei J and He C: Where, When, and How: Context-dependent functions of RNA methylation writers, readers, and erasers. Mol Cell 74: 640-650, 2019.
53. Li J, Chen K, Dong X, Xu Y, Sun Q, Wang H, Chen Z, Liu C, Liu R, Yang Z, *et al*: YTHDF1 promotes mRNA degradation via YTHDF1-AGO2 interaction and phase separation. Cell Prolif 55: e13157, 2022.